Ab Initio Chemical Kinetics for H + NCN: Prediction of NCN Heat of Formation and Reaction Product Branching via Doublet and Quartet Surfaces

ARTICLE *in* THE JOURNAL OF PHYSICAL CHEMISTRY A · JUNE 2013

Impact Factor: 2.69 · DOI: 10.1021/jp402903t · Source: PubMed

4 AUTHORS, INCLUDING:

Lyudmila V Moskaleva
Universität Bremen
57 PUBLICATIONS **997** CITATIONS
SEE PROFILE

Hui-Lung Chen
Chinese Culture University
64 PUBLICATIONS **441** CITATIONS
SEE PROFILE

THE JOURNAL OF PHYSICAL CHEMISTRY A

Article

pubs.acs.org/JPCA

Ab Initio Chemical Kinetics for H + NCN: Prediction of NCN Heat of Formation and Reaction Product Branching via Doublet and Quartet Surfaces

Wen-Shuang Teng,[†] Lyudmila V. Moskaleva,[‡] Hui-Lung Chen,*[,†] and M. C. Lin*[,⊥,§]

[†]Department of Chemistry and Institute of Applied Chemistry, Chinese Culture University, Taipei 111, Taiwan

[‡]Institut für Angewandte und Physikalische Chemie, Universität Bremen, 28359 Bremen, Germany

[⊥]Department of Chemistry, Emory University, Atlanta, Georgia 30322, United States

[§]Department of Applied Chemistry and Institute of Molecular Science, National Chiao Tung University, Hsinchu 30010, Taiwan

Supporting Information

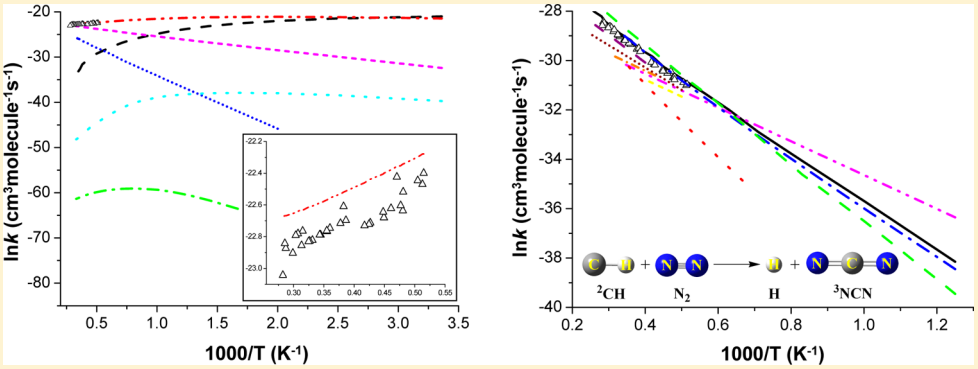

ABSTRACT: The reaction of NCN with H atoms has been investigated by *ab initio* MO and RRKM theory calculations. The mechanisms for formation of major products on the doublet and quartet potential energy surfaces have been predicted at the CCSD(T) level of theory with the complete basis set limit. In addition, the heat of formation for NCN predicted at this rigorous level and those from five isogyric reactions are in close agreement with the best value based on the isodesmic process, ^{3}CCO + N_2 = ^{3}NCN + CO, 109.4 kcal/mol, which lies within the two existing experimental values. The rate constants for the three possible reaction channels, H + NCN → CH + N_2 (k_{P1}), HCN + ^{4}N (k_{QP1}), and HNC + ^{4}N (k_{QP2}), have been calculated in the temperature range 298−3000 K. The results show that k_{P1} is significantly higher than k_{QP1} and k_{QP2} and that the total rate constant agrees well with available experimental values in the whole temperature range studied. The kinetics of the reverse CH + N_2 reaction has also been revisited at the CCSD(T)/CBS level; the predicted total rate constants at 760 Torr Ar pressure can be represented by $k_r = 4.01 \times 10^{-15}\ T^{0.90} \exp(-17.42\ \text{kcal mol}^{-1}/RT)\ \text{cm}^3\ \text{molecule}^{-1}\ \text{s}^{-1}$ at T = 800−4000 K. The result agrees closely with the most recent experimental data and the best theoretical result of Harding et al. (*J. Phys. Chem. A* **2008**, *112*, 522) as well as that of Moskaleva and Lin (*Proc. Combust. Inst.* **2000**, *28*, 2393) evaluated with a steady-state approximation after a coding error correction made in this study.

1. INTRODUCTION

The spin-forbidden process, CH($^2\Pi$) + N_2 → HCN + N(^{4}S), first proposed by Fenimore in 1971 to be one of kinetically feasible processes which could be fast enough to account for prompt NO formation in the primary zone of hydrocarbon−air flames,[1] was shown to be at least 2 orders of magnitude slower than the experimental kinetic data,[2−5] based on high-level quantum-chemical and statistical-theory calculations by Cui et al. in 1999.[6] The difficulty was soon resolved by Lin and co-workers[7,8] who predicted the existence of the spin-allowed doublet low-energy path giving rise to H + NCN radical products via a multistep isomerization from the initial ring-adduct, -C(H)NN-, to the HNCN radical intermediate. Their predicted rate constants for the production of NCN and its potential ensuing reactions involving H and CH_x (x = 1−3) radicals, based on the energetics computed at the G2M level of theory,[7,8] were shown to be able to account reasonably for the decay rates of CH radicals measured by Hanson and co-workers[4] and the formation rates of N atoms detected by Lindackers et al.[5] in their respective high-temperature shock tube studies. Since the publication in 2000 of the new prompt NO mechanism,[7,8] which will be referred to as the FML (Fenimore−Moskaleva−Lin) mechanism hereafter, NCN has been detected in shock-heated mixtures of N_2 and C_2H_6 (or

Received: March 25, 2013
Revised: June 7, 2013
Published: June 11, 2013

   dx.doi.org/10.1021/jp402903t | *J. Phys. Chem. A* 2013, 117, 5775−5784

acetic anhydride) above 2000 K[9] and in several hydrocarbon−air flame experiments[10,11] attributable to CH + N_2; the validity of our potential energy surface for NCN formation from the reaction has also been confirmed by other theoretical calculations.[12,13]

In the high-temperature shock tube studies of CH + N_2 kinetics, hydrocarbon molecules such as C_2H_6 were typically employed as CH radical precursors through their successive thermal decomposition reactions, producing mixtures of H atoms and CH_x (x = 1−3) radicals. The presence of these reactive species unavoidably affects the quantitative interpretation of experimentally measured CH decay rates and/or N and NCN radical production rates. In the modeling of measured CH and NCN concentration profiles by Hanson and coworkers[9] in shock-heated mixtures of C_2H_6 and Ar, and by Lamoureux et al.[11] in a fuel rich CH_4−O_2−N_2 flame and a stoichiometric C_2H_2−O_2−N_2 flame, the effects of H + NCN have been reported. The former group determined the rate constant for H + NCN to be $4.22 \times 10^{-11} \sim 5.73 \times 10^{-11}$ cm^3 mol^{-1} s^{-1} in the narrow temperature range of 2378−2492 K with an estimated error of ±100%. The values are consistent with the rate constant predicted by Moskaleva.[7,14] In the latter flame studies, a similar but temperature independent value, 4.2×10^{-11} cm^3 mol^{-1} s^{-1}, was reported. Very recently, Lamoureux et al.[15] also reported the first absorption spectrum at high temperature (1660 K) measured by CRDS between 329 and 329.3 nm in a rich low-pressure C_2H_2−O_2−N_2 flame. The experimental absorption spectrum, compared to the LIF and simulated spectra, demonstrates that the principal intense feature at 329.13 nm is indubitably assignable to NCN. El Bakali et al.[16] had earlier simulated CH and NO concentration profiles in several hydrocarbon flames and analyzed the effects of NCN reactions in flames with H and other reactive species, whose kinetics had been predicted by Zhu et al.[17−19]

The emergence of NCN as one of the key intermediates of prompt NO formation by the FML mechanism has motivated recent experimental work on NCN chemistry. Several high-temperature studies of NCN related kinetics were carried out by Friedrichs and associates.[20−22] Their advancement in quantitative detection of NCN behind shock waves in the parts per million (ppm) range opens a straightforward way to NCN detection in flames and to direct high-temperature rate constant measurements of NCN reactions much needed for implementation in the detailed combustion mechanisms.

Theoretically, Moskaleva[14] noted that in the H + NCN reaction, unlike its reverse CH + N_2 process, a quartet surface can be accessed without the need for kinetically rate-limiting surface crossing. Thus, what is the contribution of the quartet surface reaction to the overall rate constant of H + NCN in addition to the known doublet surface,[7,8,12,13] and what is the relative rate for H attacking a terminal N atom vs H attacking the central C atom respectively producing the HNC and HCN isomers? Another factor which affects strongly the rate of H + NCN production from CH + N_2 is the heat of formation of NCN. As the process is endothermic without an intrinsic barrier, the rate constant for NCN production is mainly enthalpically controlled. The heat of formation of NCN determined experimentally has a large deviation between the two reported values: 111.38 ± 0.69[23] and 107.4 ± 3.2 kcal/mol.[24] In this work, we shall attempt to utilize a series of isogyric and isodesmic reactions to help determine the best value which can rationalize existing experimental kinetic data for H + NCN[9,11] and those of the reverse CH + N_2 reactions.[2−5,9,11]

2. COMPUTATIONAL METHOD

With the Gaussian 09 computational chemistry software[25] we performed molecular-orbital calculations involving density-functional theory with Becke's three-parameter (B3) exchange functional and the Lee−Yang−Parr (LYP) correlation functional (B3LYP)[26,27] using a 6-311++G(3df,2p) basis set. Frequency calculations were performed at the same level to check whether the obtained equilibrium structures are local minima or saddle points, among which the reactants, intermediates, and products possess all real frequencies, whereas transition states have only one imaginary frequency. Zero-point vibrational energy (ZPE) corrections are also computed at the B3LYP/6-311++G(3df,2p) level. Intrinsic reaction coordinate (IRC)[28] calculations were also performed to confirm the connection between the transition state and the designated intermediates. To obtain reliable energies, we performed single-point calculations employing a coupled-cluster technique with single and double excitations and evaluations by perturbation theory of triple contributions CCSD(T)[29,30] based on those geometries optimized at the B3LYP/6-311++G(3df,2p) level. Further calculations were made to extrapolate the CCSD(T) results to the complete basis set limit by fitting the results obtained from different aug-cc-PVnZ basis sets and extrapolating to $n \rightarrow \infty$. For this purpose, the "cardinal number" X was introduced, where X = 2, 3, 4, and 5 for n = D, T, Q, and 5, respectively. For the extrapolation to the complete basis set limit, we used the two-parameter exponential model,[31] $E = a + b(X + 1)^{-4}$, to fit the data points. The highest level of theory used in this work is thus denoted as CCSD(T)/CBS//B3LYP/6-311++G(3df,2p). Unless otherwise specified, the CCSD(T)/CBS single-point energies are used in the following discussion. The rate constants and branching ratios for the key product channels were computed with the variational transition-state theory (TST) and Rice−Ramsperger−Kassel−Marcus (RRKM) theory[32,33] using the VariFlex program.[34]

3. RESULTS AND DISCUSSION

3.1. Heat of Formation of NCN. The best experimental values for the heat of formation of ^{3}NCN existing today, 111.38 ± 0.69 kcal/mol[23] and 107.4 ± 3.2 kcal/mol,[24] differ by as much as 4 kcal/mol. The difference, as will be illustrated later, significantly affects the rate of NCN production from CH + N_2. To ascertain the present computational approach, we calculated the geometrical parameters and thermochemical data of the NCN radical. The C−N bond length and singlet−triplet splitting energy of NCN radical predicted by the hybrid density-functional B3LYP method with a modest 6-311++G(3df,2p) basis set are 1.224 Å and 1.02 eV, respectively; they are in satisfactory agreement with experimental values (1.232 Å and 1.01 eV).[24] For the evaluation of heats of formation from heats of reaction, it is desirable to use well-balanced (isodesmic or at least isogyric)[35−38] reactions whenever possible, so as to achieve the cancellation of errors inherent in the calculation for different types of molecular structures. The current state-of-the-art procedure for obtaining highly accurate heats of formation is the application of basis set extrapolation techniques combined with coupled-cluster methodology.

dx.doi.org/10.1021/jp402903t | J. Phys. Chem. A 2013, 117, 5775−5784

Table 1. Isogyric Reactions Used To Calculate the Heats of Formation of the ^{3}NCN Molecule[a]

reaction	$\Delta_{rxn}H°$ (kcal mol^{-1})			$\Delta_fH°$ of NCN (kcal mol^{-1})			
	AVTZ[c]	AVQZ[c]	CBS limit[d]	AVTZ[c]	AVQZ[c]	CBS limit[d]	lit.
$H + {}^3NCN \rightarrow CH + N_2$ (1)	−19.33	−19.46	−19.54	108.97	109.10	109.18	111.0[e]
$^3NCN + OH \rightarrow HCN + NO$ (2)	−61.21	−63.16	−64.22	105.93	107.88	108.94	109.18[f]
$^3NCN + O_2 \rightarrow NCO + NO$ (3)	−53.41	−55.22	−56.18	105.39	107.20	108.16	111.38 ± 0.69[g]
$^3NCN + NO \rightarrow NCO + N_2$ (4)	−96.76	−98.68	−99.73	105.78	107.70	108.75	107.4 ± 3.2[h]
$^3NCN + NO_2 \rightarrow NCO + N_2O$ (5)	−65.00	−66.35	−67.28	107.36	108.71	109.64	112.98[i]
$^3CCO + N_2 \rightarrow {}^3NCN + CO$ (6)	−9.51	−9.14	−8.89	108.82	109.19	109.44	108.1 ± 0.7[j]
$^1CCO + N_2 \rightarrow {}^1NCN + CO$ (7)	0.95	1.12	1.23	134.34	134.51	134.62	130.69 ± 3.2 ∼ 136.27[k]

[a]Heats of reactions are evaluated using different basis sets at the CCSD(T) level.[b] Some experimental data from the literature are also listed. [b]All energies were evaluated using geometries optimized at the B3LYP/6-311++G(3df,2p) level. [c]AVTZ = aug-cc-PVTZ and AVQZ = aug-cc-PVQZ. [d]The two-parameter exponential model, $E = a + b(X + 1)^{-4}$, was used to fit the complete basis set limit. [e]References 7 and 8. [f]Reference 12. [g]Reference 23. [h]Reference 24. [i]Reference 39. [j]Reference 40. [k]Reference 42.

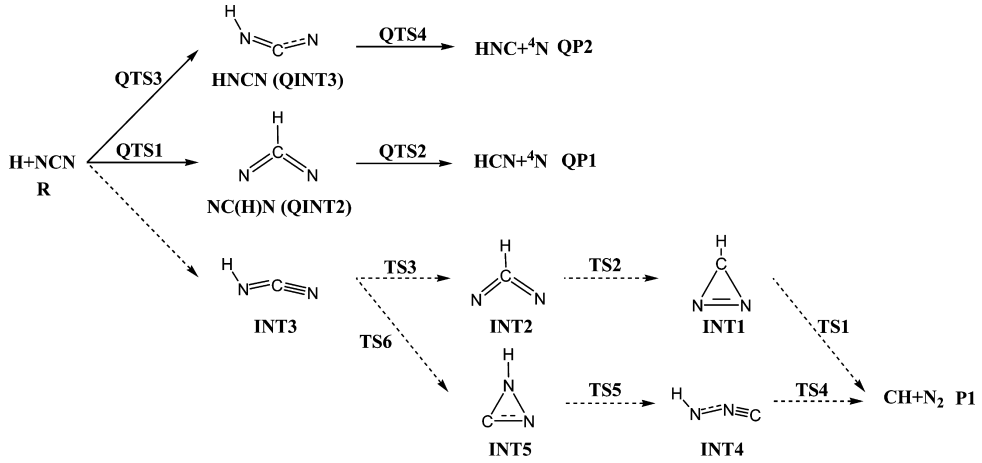

Figure 1. Schematic diagram of proposed paths for the $^2H + {}^3NCN$ reaction. Dotted and solid lines represent doublet and quartet subsurfaces.

In Table 1, we present the predicted heats of formation of ^{3}NCN radical from several model reaction energies computed at the CCSD(T) level of theory using large basis sets (including aug-cc-PVTZ, aug-cc-PVQZ, and the complete basis set limit), along with specific experimental data from the literature. A good test for correlation balance is provided by the comparison of the results obtained at different correlation levels. For an ideally balanced reaction, all errors should cancel out; thus, a less scattered set of values should indicate a better balance. According to this criterion, the values of the $\Delta_fH°$ predicted for reactions 1, 5, and 6 (Table 1) show the lowest scatter of values with respect to increasing the basis set size, indicative of the good balance (however, for reaction 1, the agreement seems to be coincidental because, as shown earlier, the calculated enthalpy of this reaction is quite sensitive to the level of theory employed).[8] As shown in Table 1, the values of $\Delta_fH°$ predicted for reactions 1, 2, 3, 4, 5, and 6 with the CBS limit are respectively 109.18, 108.94, 108.16, 108.75, 109.64, and 109.44 kcal/mol, which are close to the reported experimental values 111.38 ± 0.69 kcal/mol[20] and 107.4 ± 3.2 kcal/mol[21] and other values computed from experimental thermodynamic results 112.98 kcal/mol[39] and 108.1 ± 0.7 kcal/mol.[40] The average of our computed values using model reactions given in Table 1 is 109.01 ± 0.61 kcal/mol, which is very close to the value of 109.44 kcal/mol obtained by the isodesmic calculation from reaction 6, considered by the authors as most reliable, and also close to the computed result 109.18 kcal/mol by Harding and Klippenstein,[12] who estimated the heat of reaction for $H + {}^3NCN \rightarrow CH + N_2$ to be −19.54 kcal/mol by multireference second-order perturbation theory, CASPT2, combined with CCSD(T)/CBS single-point calculations. The value agrees exactly with our result presented in Table 1 (reaction 1). Accordingly, the heat of formation for ^{3}NCN predicted with the isodesmic reaction, 109.4 kcal/mol, may be considered as quite reliable. We mention that in an earlier work of Moskaleva and Lin on the energetics of NCN isomers[8] a very similar value, 109.1 kcal/mol, was computed at the G2M level, using a somewhat different set of model reactions. Note that G2M is a modified G2 model chemistry providing an approximation to the RCCSD(T)/6-311++G(3df,2p) electronic energy.[41] That earlier estimation had nevertheless a relatively large uncertainty of ±1.5 kcal/mol. Significantly, from reaction 1, the G2M method yields the NCN heat of formation as high as 111.1 kcal/mol, even outside the upper value of the given interval. In contrast, the current CCSD(T)/CBS approach gives a much smaller scatter of the calculated values of $\Delta_fH°$ (NCN) from the different model reactions, ca. 1.5 kcal/mol (Table 1). It should be noted that the $\Delta_fH°$ values predicted with the AVTZ and AVQZ basis sets for the same set of reactions in the table yield a broader range of values, ca. 4.5 and 2.0 kcal/mol, respectively. Thus, the extrapolation to the CBS limit seems to be the key to the success of our CCSD(T)/CBS methodology.

dx.doi.org/10.1021/jp402903t | J. Phys. Chem. A 2013, 117, 5775−5784

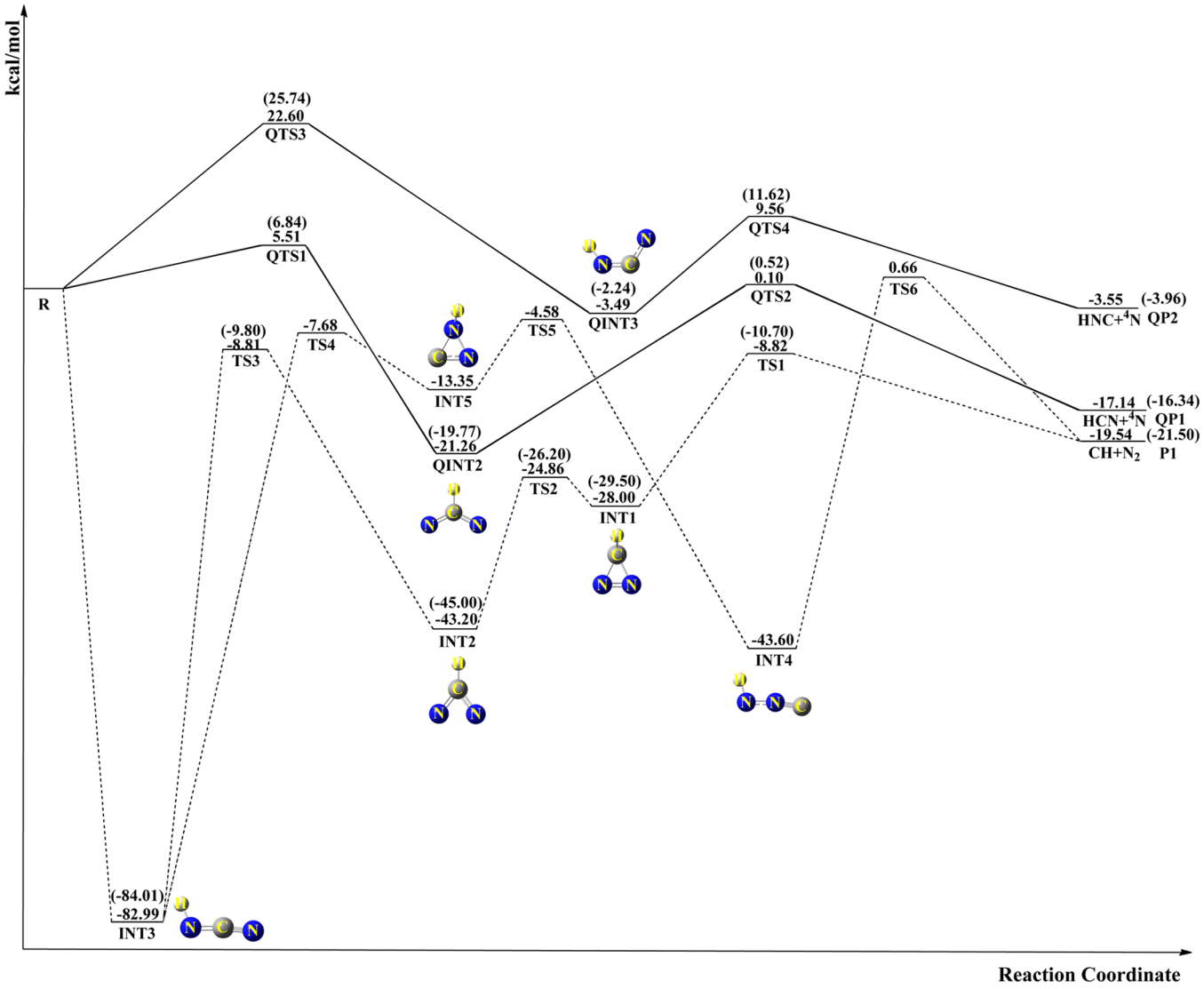

Figure 2. Calculated profiles on the potential energy surface for possible paths of the $^2H + {}^3NCN$ reaction. Dotted and solid lines represent doublet and quartet subsurfaces at the level of CCSD(T)/CBS//B3LYP/6-311++G(3df,2p). The data in parentheses are from our previously published work.[7,8]

As the heat of formation of ^1CCO is also known from the study of Neumark and co-workers,[42] we have accordingly predicted the heat of formation of ^1NCN using the isodesmic reaction $^1CCO + N_2 \rightarrow {}^1NCN + CO$. A number of different basis sets are also employed for comparison, including aug-cc-PVTZ, aug-cc-PVQZ, and the CBS limit as listed in Table 1 (reaction 7). The predicted results are quite consistent; the deviation between the CCSD(T)/CBS (134.62 kcal/mol) and experimental values (130.69 ± 3.2∼136.27 kcal/mol) is less than ca. 1.7−3.9 kcal/mol. The CCSD(T)/CBS//B3LYP/6-311++G(3df,2p) method appears to be quite reliable and is thus suitable for evaluation of the H + NCN kinetics and that of its reverse process.

3.2. Potential Energy Surfaces and Rate Constant Calculations for H + NCN with Doublet and Quartet Configurations. The doublet and quartet schematic diagrams of the key paths for NCN reactions with H atoms are depicted in Figure 1, in which the names and numbers of intermediates and transition states used here are consistent with our previously published work for the same structures using the G2M composite scheme.[7,8,14] The profile of the doublet and quartet PESs calculated at the CCSD(T)/CBS//B3LYP/6-311++G(3df,2p) level is shown in Figure 2, and the calculated energetics for the doublet and quartet species are tabulated in Table 2 (including our previously published data), in which the ZPE corrections and the energies with respect to the reactants (H + NCN) calculated at the CCSD(T)/CBS level, denoted as CRE, are presented. The optimized geometries for the doublet and quartet species involved in the H + NCN reaction at the B3LYP/6-311++G(3df,2p) level are shown in Figures S1 and S2 (Supporting Information).

3.2.1. Doublet Surface. On the doublet surface, shown in Figure 1 by dotted paths, the H + NCN reaction may first form the primary adduct HNCN (**INT3**), which is energetically more stable than the reactants by 82.99 kcal/mol. After the formation of **INT3**, there are two distinct paths for formation of the final products CH + N_2. Along the energetically most favorable path, the **INT3** can undergo a simple H-shift transition state, **TS3**, lying 8.82 kcal/mol below the reactants, forming a quasi-cyclic intermediate **INT2** with an exothermicity of 43.20 kcal/mol. The reaction may proceed further through isomerization from **INT2** to **INT1** via **TS2** with a barrier of

dx.doi.org/10.1021/jp402903t | J. Phys. Chem. A 2013, 117, 5775−5784

Table 2. ZPE (hartree), Total Energies (TE, hartree), and Relative Energies (RE, kcal/mol) of Reactants, Intermediates, Transition States, and Products Calculated at the CCSD(T)/CBS//B3LYP/6-311++G(3df,2p) Level (CTE and CRE) for the H + NCN System[a]

	ZPE[b]	CTE + ZPE	CRE[c]	Moskaleva[e]
R(H+NCN)	0.008506	−147.806644	00.00	0.00
INT1	0.019301	−147.851259	−28.00	−29.50
INT2	0.019485	−147.875485	−43.20	−45.00
INT3	0.019610	−147.938900	−82.99	−84.01
INT4	0.019409	−147.876131	−43.60	
INT5	0.018971	−147.827919	−13.35	
QINT3	0.018355	−147.812205	−3.49	−2.24
QINT2	0.017780	−147.840530	−21.26	−19.77
TS1	0.014276	−147.820694	−8.82	−10.70
TS2	0.017292	−147.846258	−24.86	−26.20
TS3	0.015554	−147.820686	−8.81	−9.80
TS4	0.014835	−147.805595	0.66	
TS5	0.016798	−147.813942	−4.58	
TS6	0.016112	−147.818888	−7.68	
QTS1	0.009912	−147.797868	5.51	6.84
QTS2	0.016353	−147.806487	0.10	0.52
QTS3	0.010055	−147.770635	22.60	25.74
QTS4	0.015862	−147.791408	9.56	11.62
P1 (CH + N_2)	0.012021	−147.837789	−19.54	−21.50
QP1 (HCN + N)	0.016308	−147.833952	−17.14	−16.34
QP2 (HNC + N)	0.014552	−147.812298	−3.55	−3.96

[a]The data of our previously published work are also included. [b]Zero-point energy (au) at the B3LYP/6-311++G(3df,2p) level. [c]Relative energy (kcal/mol) with respect to the reactants. [d]The two-parameter exponential model, $E = a + b(X + 1)^{-4}$, was used to fit the complete basis set limit. [e]References 7 and 14.

18.34 kcal/mol by shortening the N−N bond from 1.566 Å in **INT2** to 1.244 Å in **INT1**. Finally, the cyclic intermediate **INT1** can overcome an activation barrier of 19.19 kcal/mol at **TS1** by stretching its C−N bonds to ca. 1.59 Å to produce **P1** (CH + N_2), with an exothermicity of 19.54 kcal/mol. It is evident from Figure 2 that the G2M relative energies with respect to H + NCN calculated in our earlier study[7] are consistently lower by ca. 1.0−2.0 kcal/mol than the present CCSD(T)/CBS values. Along the less favorable reaction path, the **INT3** adduct can cyclize via **TS4** (lying 7.68 kcal/mol below the reactants) to form a three-membered ring intermediate, **INT5**, and proceed further by passing over two energy barriers (−4.58 and 0.66 kcal/mol for **TS5** and **TS6**, respectively) to open the ring by breaking a C−N bond, to be followed by a simple H-shift from N atom to the C atom to produce **P1** (CH + N_2).

3.2.2. Quartet Surface. On the quartet surface, shown in Figure 1 by solid paths, the H + NCN reaction may generate the following possible products with the predicted enthalpy changes: HCN + ^{4}N (**QP1**), −17.14 kcal/mol and HNC + ^{4}N (**QP2**), −3.55 kcal/mol. The former channel results from H addition to the central C atom, whereas the latter from H addition to the N site of NCN. The most favorable reaction path is **R** → **QTS1** → **QINT2** → **QTS2** → **QP1**, with the highest energy barrier at **QTS1**, 5.51 kcal/mol, having an overall exothermicity of 17.14 kcal/mol. Because **QTS2** lies only 0.1 kcal/mol above the reactants, clearly, **QTS1** is expected to be rate-controlling. On the other hand, the energetically less competitive product **QP2** (HNC + ^{4}N) could be formed via the path **R** → **QTS3** → **QINT3** → **QTS4** → **QP2**, with the highest activation barrier at **QTS3**, 22.60 kcal/mol, and an overall exothermicity of 3.55 kcal/mol. Both reaction paths on the quartet PES have been previously addressed by Moskaleva at the G2M level.[14] G2M relative energies with respect to H + NCN are consistently somewhat higher than the current CCSD(T)/CBS values, though the differences in most cases do not exceed ca. 1.5 kcal/mol. Only for the energetically high lying **QTS3** and **QTS4** are the deviations of G2M energies larger, ca. 3.1 and 2.0 kcal/mol, respectively. Even though the relative energies of each stationary point on the quartet surface are mostly higher than those on the doublet surface, the former pathway with the quartet configuration may become competitive at higher temperatures.

3.2.3. Rate Constant Calculations. Variational TST and RRKM calculations have been carried out for this reaction with the VariFlex code[34] including the doublet and quartet reaction channels (omitting kinetically irrelevant intermediate steps) shown as follows:

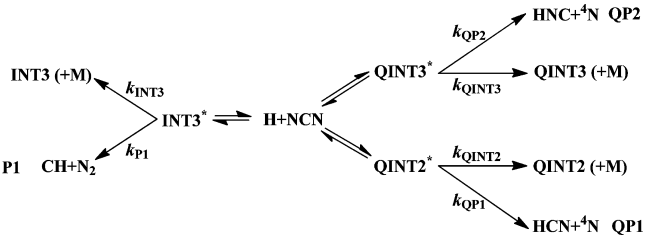

In the above scheme we ignored the effect of INT4 and INT2 in our prediction of the rate constants for $CH_2 + N_2$ → H + NCN in both directions. The well depths of those intermediates, which appear in paths A and B, respectively, are much shallower than that of HNCN. In addition, under the prompt NO formation condition in flames above 1500 K, the effect of pressure is negligible and the values of rate constants for both forward and reverse directions are controlled mainly by the variational transition states near the dissociation threshold H···NCN. In the original work of Moskaleva and Lin,[7] treated by the steady-state method, the INT2 was included in their canonical RRKM calculation, while, in the work of Harding and Klippenstein,[12] by solving the master equation, INT2 was also ignored in the rate-constant calculation, similar to the present work. The results of the three calculations, as will be shown later, all agree closely with existing experimental data. The energies used in the calculation are plotted in Figure 2, and the vibrational frequencies and moments of inertia are listed in Table S1. The Lennard-Jones (LJ) parameters employed in the calculation are as follows: for Ar,[43] σ = 3.465 Å, ε/k = 113.50 K, and for HNCN,[14] σ = 4.560 Å, ε/k = 48.20 K. For the variational rate constant calculations by the VariFlex code, a statistical treatment of the transitional-mode contributions to the transition-state partition functions is performed variationally. The energy-transfer process was computed on the basis of the exponential down model with a $\langle \Delta E \rangle_{down}$ value (the mean energy transferred per collision) of 400 cm^{-1} for Ar. In addition, the estimate of the transitional-mode contribution to the transition-state number of states for a given energy was evaluated via Monte Carlo integration with 10000 configuration numbers. In order to achieve convergence in the integration over the energy range, an energy grain size of 120 cm^{-1} was used. The total angular momentum J covered the

dx.doi.org/10.1021/jp402903t | J. Phys. Chem. A 2013, 117, 5775−5784

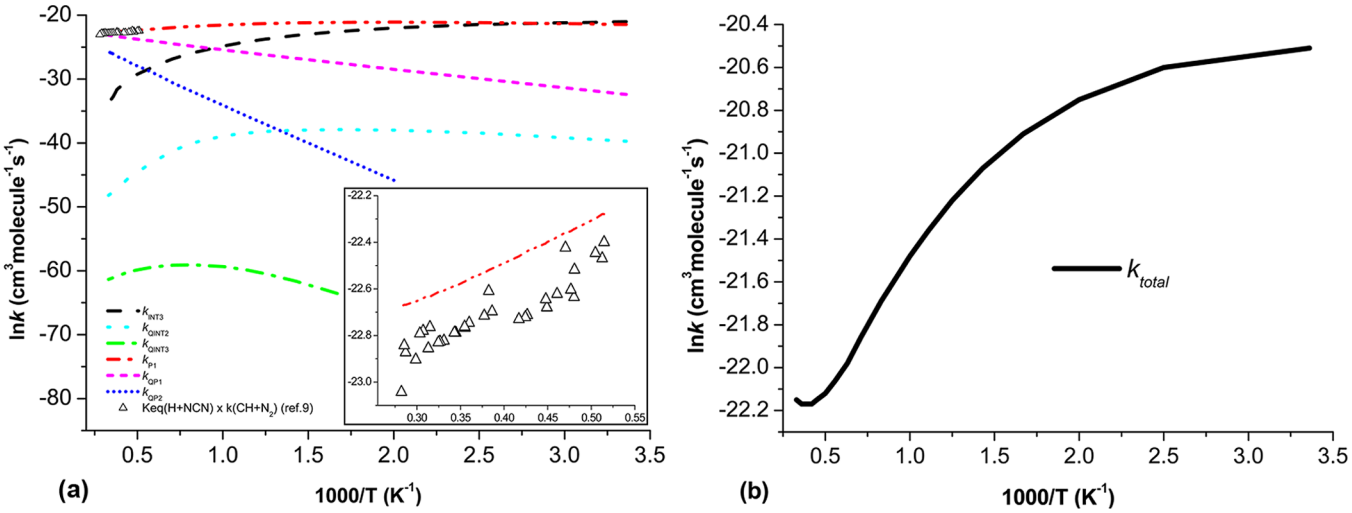

Figure 3. Predicted rate constants of (a) k_{INT3}, k_{QINT2}, k_{QINT3}, k_{P1}, k_{QP1}, k_{QP2}, and converted experimental values from ref 9; (inset) expanded view of the high T region of the graph; and (b) the total rate constants ($k_{total} = k_{INT3} + k_{QINT2} + k_{QINT3} + k_{P1} + k_{QP1} + k_{QP2}$) at Ar pressure of 760 Torr in the temperature range of 298−3000 K.

range from 1 to 250 in steps of 10 for the E, J-resolved calculation.

The predicted values for individual rate constants (k_{INT3}, k_{QINT2}, k_{QINT3}, k_{P1}, k_{QP1}, and k_{QP2}) and total rate constants ($k_{total} = k_{INT3} + k_{QINT2} + k_{QINT3} + k_{P1} + k_{QP1} + k_{QP2}$) for reaction of H + NCN at 760 Torr Ar pressure in the temperature range of 298−3000 K are shown in parts a and b, respectively, of Figure 3. As we can see from Figure 3a, the values of k_{INT3} and k_{QINT2} substantially decrease as the temperature increases from 298 to 3000 K, indicating that collisional deactivation giving **INT3** and **QINT2** becomes increasingly less competitive at higher temperatures. In addition, the calculated results reveal that the rate constant k_{P1} giving CH + N_2 via the doublet paths is more favorable than k_{QP1} and k_{QP2} of the quartet paths in the whole temperature range. In order to further ascertain the computational approach used in rate constant predictions, we also separately calculated the equilibrium constant K_{eq} for H + NCN → CH + N_2 to convert the experimental rate constants of Vasudevan et al.[9] for CH + N_2 → H + NCN to those for H + NCN → CH + N_2; the results given by open triangles are also presented in Figure 3a. From the figure it is evident that our predicted values of k_{P1} are in reasonable agreement with the converted experimental results in the temperature range of 1943−3543 K. It is also clear from the expanded inset of the figure that the H + NCN → CH + N_2 has negative temperature dependence, at least in the temperature range studied. Second, there is a small (∼15%) deviation between theory and experiment which may be attributed in part to the theoretical overprediction and in part to the large error (estimated to be ±25% at ∼3350 K and ±35% at ∼2100 K[9]) from the modeling of the measured CH profiles involving the complex CH_x and NCN reactions unavoidably present in the complex chemical system, as alluded to before.

The branching ratios for the four primary reaction channels on the doublet and quartet surfaces (k_{INT3}, k_{P1}, k_{QP1}, and k_{QP2}) at 760 Torr Ar pressure in the temperature range of 298−3000 K are shown in Figure 4. The stabilization rate constant k_{INT3} in the low-temperature range of 298−350 K clearly has the largest value, accounting for 0.61−0.49 of the total rate. However, at higher temperatures (350−1100 K), CH + N_2 (**P1**) formation becomes dominant, accounting for 0.49−0.95 of the total rate.

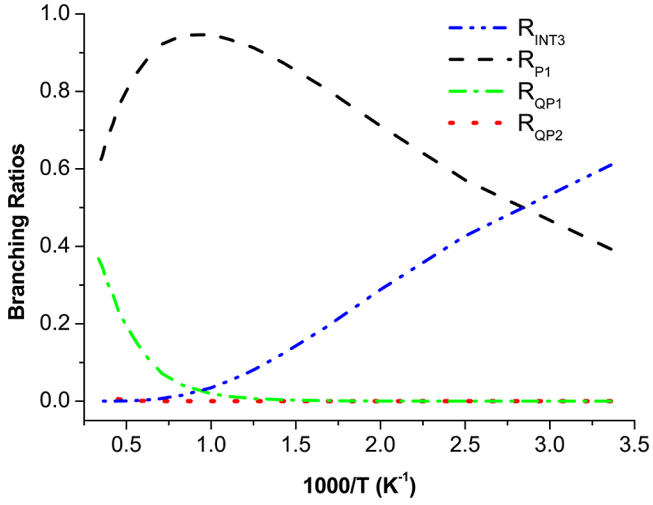

Figure 4. Predicted branching ratios for the principal reaction channels of H + NCN reactions at 760 Torr Ar pressure in the temperature range of 298−3000 K.

Besides, it is also clear that the formation of HCN + ^{4}N (**QP1**) becomes more competitive as the temperature goes beyond 1100 K.

We summarize the rate expressions for each individual rate constant (k_{INT3}, k_{QINT2}, k_{QINT3}, k_{P1}, k_{QP1}, and k_{QP2}) at seven specific pressures between 5 Torr and 100 atm in the temperature range of 298−3000 K in Table 3. In this temperature range, the values of k_{INT3}, k_{QINT2}, and k_{QINT3} have strong pressure dependencies, as one would expect; the values of k_{P1}, k_{QP1}, and k_{QP2}, however, are pressure independent below 100 atm. The predicted total rate constant, k_{total}, at 760 Torr Ar pressure can be represented by the following: $k_{total} = (7.68 \times 10^{-8})T^{-0.75} \exp(0.16 \text{ kcal mol}^{-1}/RT)$ at T = 298−3000 K, in units of cm^3 molecule^{-1} s^{-1}. Comparison with the previous experimental and computational values has also been made (as shown in Table 4 and Figure 5); the predicted specific rate constants at different temperatures (2378, 2420, 2455, 2491, and 2492 K) with the corresponding pressures 0.421, 0.413, 0.437, 0.401, and 0.447 atm for the H + NCN → HCN + N reaction (k_{QP1}) vary within the small range of values, 6.60

dx.doi.org/10.1021/jp402903t | J. Phys. Chem. A 2013, 117, 5775−5784

Table 3. Predicted Rate Equations[a] of k_{INT3}, k_{QINT3}, k_{QINT2}, k_{P1}, k_{QP1}, and k_{QP2} at the Ar Pressures of 5 Torr, 100 Torr, 380 Torr, 760 Torr, 10 atm, 50 atm, and 100 atm in the Temperature Range of 298−3000 K for the H + NCN Reaction

reaction	P	A	n	B
k_{INT3}	5 Torr	7.07×10^{12}	−9.03	−4.42
	100 Torr	2.95×10^{17}	−9.58	−5.25
	380 Torr	3.86×10^{18}	−9.50	−6.19
	760 Torr	2.98×10^{18}	−9.28	−6.56
	10 atm	5.89×10^{15}	−7.99	−6.95
	50 atm	5.35×10^{12}	−6.86	−6.60
	100 atm	1.52×10^{11}	−6.32	−6.30
k_{QINT2}	5 Torr	6.52×10^{18}	−11.85	−13.38
	100 Torr	2.29×10^{20}	−11.90	−13.22
	380 Torr	2.22×10^{21}	−12.00	−13.10
	760 Torr	1.04×10^{22}	−12.08	−13.07
	10 atm	2.78×10^{25}	−12.61	−13.56
	50 atm	1.92×10^{28}	−13.02	−14.89
	100 atm	1.14×10^{29}	−13.05	−15.56
k_{QINT3}	5 Torr	2.49×10^{9}	−10.44	−28.42
	100 Torr	5.41×10^{10}	−10.45	−28.36
	380 Torr	2.80×10^{11}	−10.48	−28.28
	760 Torr	8.32×10^{11}	−10.53	−28.24
	10 atm	1.37×10^{14}	−10.82	−28.06
	50 atm	4.30×10^{16}	−11.23	−27.94
	100 atm	1.25×10^{18}	−11.50	−27.95
k_{P1}	all pressures	6.27×10^{-05}	−1.61	−1.49
k_{QP1}	all pressures	8.24×10^{-12}	0.41	−5.46
k_{QP2}	all pressures	4.75×10^{-13}	0.79	−22.24

[a]Rate constants are represented by $k = AT^n \exp(B \text{ kcal mol}^{-1}/RT)$ in units of cm^3 $molecule^{-1}$ s^{-1}.

Table 4. Predicted Rate Constants[a] for the H + NCN → HCN + N Reaction (k_{QP1}) at the He Pressures of 0.421, 0.413, 0.437, 0.401, and 0.447 atm in the Temperature Range of 2378, 2420, 2455, 2491, and 2492 K and the Corresponding Experimental Data from the Literature

T(K)	P(atm)	k_{QP1}	exp[b]
2378	0.421	6.60×10^{-11}	4.22×10^{-11}
2420	0.413	6.78×10^{-11}	5.45×10^{-11}
2455	0.437	6.93×10^{-11}	5.58×10^{-11}
2491	0.401	7.08×10^{-11}	5.73×10^{-11}
2492	0.447	7.09×10^{-11}	5.73×10^{-11}

[a]Rate constants are in units of cm^3 $molecule^{-1}$ s^{-1}. [b]Uncertainty of this data was estimated to be a factor of 2 (ref 9).

$\times 10^{-11} \sim 7.09 \times 10^{-11}$ cm^3 $molecule^{-1}$ s^{-1}, which are consistent with our previously predicted values[7] as well as with the temperature independent result, 4.2×10^{-11} cm^3 $molecule^{-1}$ s^{-1}, by Lamoureux et al.[11] in a flame study and with the kinetically modeled values from the experiment of Hanson and co-workers ($4.22 \times 10^{-11} \sim 5.73 \times 10^{-11}$ cm^3 $molecule^{-1}$ s^{-1}, with an uncertainty estimated to be a factor of 2).[9]

3.3. Rate Constant for CH + N_2 → H + NCN Revisited.

From our calculated potential energy surface, it is clear that there are two different paths for the reverse reaction CH + N_2 → H + NCN. Path A, **CH + N_2 → TS1 → INT1 → TS2 → INT2 → TS3 → INT3 → H + NCN**, was proposed in our previous computational work.[7] Another potential path, B,

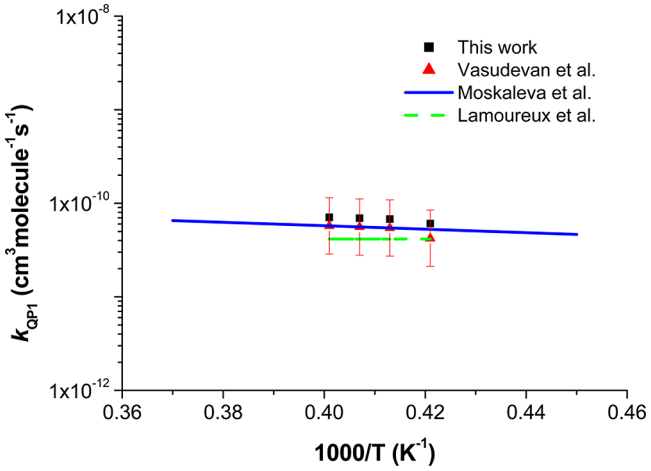

Figure 5. Rate coefficient data for H + NCN → HCN + N: solid squares, this work; red triangle, Vasudevan et al.,[9] uncertainty in their data was estimated to be a factor of 2; solid line, Moskaleva et al.;[7] and dashed line, Lamoureux et al.[11]

which follows the route **CH + N_2 → TS6 → INT4 → TS5 → INT5 → TS4 → INT3 → H + NCN**, forming the same final products, has been proposed by Berman et al.[13] and Harding and Klippenstein.[12] We compare the potential energy surface with that of Berman et al.,[13] in which the CH + N_2 reaction starts with a barrierless association to form HCNN and then proceeds through a simple H-shift transition state with a very high energy barrier, 83.6 kcal/mol, to form **INT4**. In our calculation, however, we found another more attainable transition state, **TS6**, connecting directly to the **INT4**, with a much lower activation barrier of 20.20 kcal/mol, which is very close to the 19.5 kcal/mol barrier reported by Harding and Klippenstein,[12] who indicated that the contribution from this path might increase at higher temperatures.

The predicted rate constants for the CH + N_2 reaction at an Ar pressure of 760 Torr in the temperature range of 800−4000 K are shown in Figure 6, and the rate expressions for the two paths and their sum can be represented as follows:

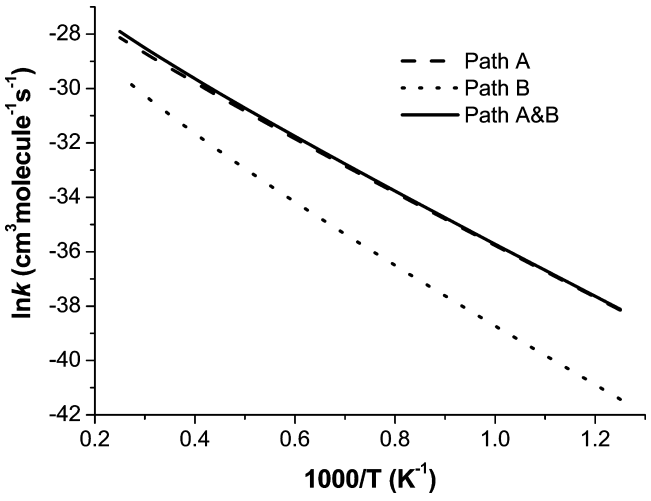

Figure 6. Predicted rate constants of the contributions from two different pathways (paths A and B) for the CH + N_2 → H + NCN reaction. The pressure is 760 Torr, and the temperature range is 800−4000 K.

dx.doi.org/10.1021/jp402903t | J. Phys. Chem. A 2013, 117, 5775−5784

- $k_A = (1.93 \times 10^{-14})T^{0.69} \exp(-17.72 \text{ kcal mol}^{-1}/RT)$ cm^3 molecule^{-1} s^{-1}
- $k_B = (2.53 \times 10^{-18})T^{1.61} \exp(-18.56 \text{ kcal mol}^{-1}/RT)$ cm^3 molecule^{-1} s^{-1}
- $k_{A\&B} = (4.01 \times 10^{-15})T^{0.90} \exp(-17.42 \text{ kcal mol}^{-1}/RT)$ cm^3 molecule^{-1} s^{-1}

in which k_A and k_B represent the individual rate constants for the formation of H + NCN via paths A and B, respectively, and $k_{A\&B}$ is the total rate constant ($k_A + k_B$). The computed results clearly show that, under the conditions studied, path A, proposed in 2000 by Moskaleva et al.,[7,8] predominates. The calculated total rate constant for CH + N_2 is compared in Figure 7 with experimental and theoretical data available in the literature[3−5,9,12,16,44] including our previously predicted value (M&L, ref 7) and the present results (this work and M&L corrected). In the course of preparation of this article, we found an error in the original RRKM code used for the calculation of the rate constant of CH + N_2,[7] which unfortunately originated from a programming typo. The old result based on the PES calculated at the G2M level of theory, which had noticeably underpredicted the NCN production rate, has now been corrected (M&L corrected), and the good agreement with the present calculation on the basis of CCSD(T)/CBS PES is evident as shown in Figure 7. Our newly predicted results based on the CCSD(T)/CBS energies with ME solution in the RRKM calculation (this work; black solid line) and the coding-error corrected based on G2M energies with the steady-state approximation in the RRKM calculation (M&L corrected; green dash line) both agree well with the most recent experimental work of Hanson and co-workers[9] and the best theoretical result from Harding and Klippenstein[12] in the temperature range of 800−4000 K. The reduction of the reaction endothermicity from 21.5 to 19.5 kcal/mol in the present work gives rise to an especially good agreement with the best experimental and theoretical results to date.

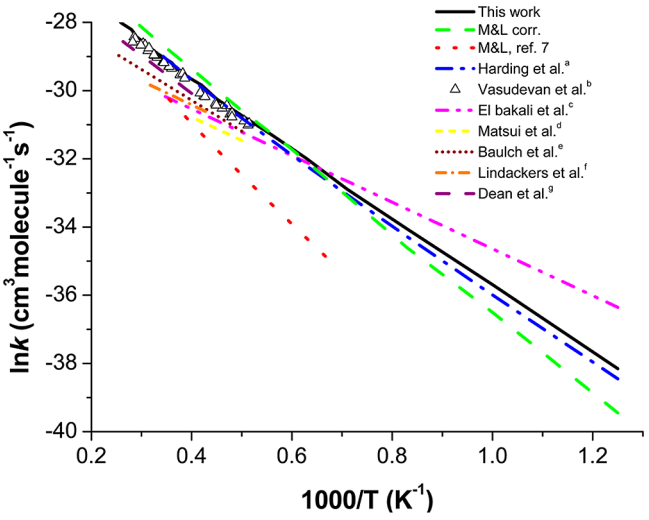

Figure 7. Plot of the theoretical predictions and experimental measurements for the CH + N_2 → H + NCN rate constant. The pressure is 760 Torr, and the temperature range is 800−4000 K.

4. CONCLUSION

The potential energy surfaces and mechanisms for the reaction of NCN with H and its reverse CH + N_2 reaction have been computed at the CCSD(T)/CBS level of theory; the rate constants for the possible reaction channels have been predicted. The predicted total rate constant for the H + NCN reaction, k_{total}, at 760 Torr Ar pressure can be represented by the following: $k_{total} = (7.68 \times 10^{-8})T^{-0.75} \exp(0.16 \text{ kcal mol}^{-1}/RT)$ cm^3 molecule^{-1} s^{-1} at T = 298−3000. The result agrees well with available experimental data ($4.22 \times 10^{-11} \sim 5.73 \times 10^{-11}$ cm^3 mol^{-1} s^{-1}). In addition, our newly predicted rate constants for the CH + N_2 reaction at 760 Torr Ar pressure in the temperature range of 800−4000 K are also given; the computed result agrees well with the most recent experimental data of Hanson and co-workers[9] and the theoretical prediction of Harding and Klippenstein,[12] as well as with that of the (corrected) earlier prediction of Moskaleva and Lin[7] using the best heat of formation of NCN obtained with the isodesmic reaction, CCO + N_2 → NCN + CO, 109.4 kcal/mol (which was shown to be in close agreement with the results predicted with five different isogyric processes).

■ ASSOCIATED CONTENT

Supporting Information

Frequencies and moments of inertia for the species involved in the reaction of H + NCN, calculated at the B3LYP/6-311++G(3df,2p) level; and calculated structural parameters of all involved stationary geometries of the H + NCN reaction at the B3LYP/6-311++G(3df,2p) level. This material is available free of charge via the Internet at http://pubs.acs.org.

■ AUTHOR INFORMATION

Corresponding Author

*E-mail: chl3@faculty.pccu.edu.tw and chemmcl@emory.edu. Tel: +886-2-28610511, ext 25313. Fax: +886-2-28617006.

Notes

The authors declare no competing financial interest.

■ ACKNOWLEDGMENTS

We would like to acknowledge support from (1) Taiwan's National Science Council for H.-L.C. (under Grant Number NSC 100-2113-M-034-002-MY2) and M.C.L. (the support from Taiwan's MOE ATU program as well as the National Science Council and the Taiwan Semiconductor Manufacturing Co. for the NSC-distinguished visiting professorship and the TSMC distinguished professorship, respectively, at the Center for Interdisciplinary Molecular Science, National Chiao Tung University), (2) the financial support by Chinese Culture University, and (3) Taiwan's National Center for High-performance Computing, for the use of computer time.

■ REFERENCES

(1) Fenimore, C. P. Formation of Nitric Oxide in Premixed Hydrocarbon Flames. *Proc. Combust. Inst.* **1977**, *13*, 373−380.

(2) Blauwens, J.; Smets, B.; Peeters, J. Mechanism of "Prompt" NO Formation in Hydrocarbon Flames. *Proc. Combust. Inst.* **1977**, *16*, 1055−1064.

(3) Matsui, Y.; Nomaguchi, T. Spectroscopic Study of Prompt Nitrogen Oxide Formation Mechanism in Hydrocarbon-Air Flames. *Combust. Flame* **1978**, *32*, 205−214.

(4) Dean, A. J.; Hanson, R. K.; Bowman, C. T. A Shock Tube Study of Reactions of Carbon Atoms and Methylidyne with Nitric Oxide Including Product Channel Measurements. *J. Phys. Chem.* **1991**, *95*, 3180−3189.

(5) Lindackers, D.; Burmeister, M.; Roth, P. Perturbation Studies of High Temperature C and CH Reactions with N_2 and NO. *Proc. Combust. Inst.* **1991**, *23*, 251−257.

(6) Cui, Q.; Morokuma, K.; Bowman, J. M.; Klippenstein, S. The Spin-Forbidden Reaction $CH(^2\Pi) + N_2 \rightarrow HCN + N(^4S)$ Revisited. II. Nonadiabatic Transition State Theory and Application. *J. Chem. Phys.* **1999**, *110*, 9469−9482.
(7) Moskaleva, L. V.; Lin, M. C. The Spin-Conserved Reaction CH + N_2→ H + NCN: A Major Pathway to Prompt NO Studied by Quantum/Statistical Theory Calculations and Kinetic Modeling of Rate Constant. *Proc. Combust. Inst.* **2000**, *28*, 2393−2401.
(8) (a) Moskaleva, L. V.; Xia, W.-S.; Lin, M. C. The CH + N_2 Reaction over the Ground Electronic Doublet Potential Energy Surface: A Detailed Transition State Search. *Chem. Phys. Lett.* **2000**, *331*, 269−277. (b) Moskaleva, L. V.; Lin, M. C. Computational Study on the Energetics of NCN Isomers and the Kinetics of the C + N_2 = N + CN Reaction. *J. Phys. Chem. A* **2001**, *105*, 4156−4163.
(9) Vasudevan, V.; Hanson, R. K.; Bowman, C. T.; Golden, D. M.; Davidson, D. F. Shock Tube Study of the Reaction of CH with N_2: Overall Rate and Branching Ratio. *J. Phys. Chem. A* **2007**, *111*, 11818−11830.
(10) Smith, G. P. Evidence of NCN as a Flame Intermediate for Prompt NO. *Chem. Phys. Lett.* **2003**, *367*, 541.
(11) Lamoureux, N.; Desgroux, P.; El Bakli, A.; Pauwels, J. F. Experimental and Numerical Study of the Role of NCN in Prompt-NO Formation in Low-Pressure CH_4−O_2−N_2 and C_2H_2−O_2−N_2 Flames. *Combust. Flame* **2010**, *157*, 1929−1941.
(12) Harding, L. B.; Klippenstein, S. J. Kinetics of CH + N_2 Revisited with Multireference Methods. *J. Phys. Chem. A* **2008**, *112*, 522−532.
(13) Berman, M. R.; Tsuchiya, T.; Gregusova, A.; Perera, A.; Bartlett, R. J. HNNC Radical and Its Role in the CH + N_2 Reaction. *J. Phys. Chem. A* **2007**, *111*, 6894−6899.
(14) Moskaleva, L. V. Ph.D. Dissertation, Emory University, 2001.
(15) Lamoureux, N.; Western, C. M.; Mercier, X.; Desgroux, P. Reinvestigation of the Spectroscopy of the $A^3\Pi_u$—$X^3\Sigma_g^-$ Transition of the NCN Radical at High Temperature: Application to Quantitative NCN Measurement in Flames. *Combust. Flame* **2013**, *160*, 755−765.
(16) El Bakali, A.; Pillier, L.; Desgroux, P.; Lefort, B.; Gasnot, L.; Pauwels, J. F.; da Costa, I. NO Prediction in Natural Gas Flames Using GDF-Kin ®3.0 Mechanism NCN and HCN Contribution to Prompt-NO Formation. *Fuel* **2006**, *85*, 896−909.
(17) Zhu, R. S.; Lin, M. C. Ab Initio Study of the Oxidation of NCN by O_2. *Int. J. Chem. Kinet.* **2005**, *37*, 593−598.
(18) Zhu, R. S.; Lin, M. C. Ab Initio Study on the Oxidation of NCN by O (^{3}P): Prediction of the Total Rate Constant and Product Branching Ratios. *J. Phys. Chem. A* **2007**, *111*, 6766−6771.
(19) Zhu, R. S.; Nguyen, H. M. T. Ab Initio Study on the Oxidation of NCN by OH: Prediction of the Individual and Total Rate Constants. *J. Phys. Chem. A* **2009**, *113*, 298−304.
(20) Dammeier, J.; Friedrichs, G. Direct Measurements of the Rate Constants of the Reactions NCN + NO and NCN + NO_2 Behind Shock Waves. *J. Phys. Chem. A* **2011**, *115*, 14382−14390.
(21) Dammeier, J.; Faßheber, N.; Friedrichs, G. Direct Measurements of the High Temperature Rate Constants of the Reactions NCN + O, NCN + NCN, and NCN + M. *Phys. Chem. Chem. Phys.* **2012**, *14*, 1030−1037.
(22) Friedrichs, G.; Dammeier, J.; Faßheber, N. Shock Tube Study on the Reactions NCN + H and NCN + O. *7th International Conference on Chemical Kinetics*; MIT, Cambridge, USA, July 2011.
(23) Bise, R. T.; Choi, H.; Neumark, D. M. Photodissociation Dynamics of the Singlet and Triplet States of the NCN Radical. *J. Chem. Phys.* **1999**, *111*, 4923−4933.
(24) Clifford, E. P.; Wenthold, P. G.; Lineberger, W. C.; Petersson, G. A.; Ellison, G. B. Photoelectron Spectroscopy of the NCN^- and $HNCN^-$ Ions. *J. Phys. Chem. A* **1997**, *101*, 4338−4345.
(25) Frisch, M. J.; Trucks, G. W.; Schlegel, H. B.; Scuseria, G. E.; Robb, M. A.; Cheeseman, J. R.; Scalmani, G.; Barone, V.; Mennucci, B.; Petersson, G. A.; Nakatsuji, H.; Caricato, M.; Li, X.; Hratchian, H. P.; Izmaylov, A. F.; Bloino, J.; Zheng, G.; Sonnenberg, J. L.; Hada, M.; Ehara, M.; Toyota, K.; Fukuda, R.; Hasegawa, J.; Ishida, M.; Nakajima, T.; Honda, Y.; Kitao, O.; Nakai, H.; Vreven, T.; Montgomery, J. A., Jr.; Peralta, J. E.; Ogliaro, F.; Bearpark, M.; Heyd, J. J.; Brothers, E.; Kudin, K. N.; Staroverov, V. N.; Kobayashi, R.; Normand, J.; Raghavachari, K.; Rendell, A.; Burant, J. C.; Iyengar, S. S.; Tomasi, J.; Cossi, M.; Rega, N.; Millam, N. J.; Klene, M.; Knox, J. E.; Cross, J. B.; Bakken, V.; Adamo, C.; Jaramillo, J.; Gomperts, R.; Stratmann, R. E.; Yazyev, O.; Austin, A. J.; Cammi, R.; Pomelli, C.; Ochterski, J. W.; Martin, R. L.; Morokuma, K.; Zakrzewski, V. G.; Voth, G. A.; Salvador, P.; Dannenberg, J. J.; Dapprich, S.; Daniels, A. D.; Farkas, Ö.; Foresman, J. B.; Ortiz, J. V.; Cioslowski, J.; Fox, D. J. *Gaussian 09*, Revision A.1; Gaussian, Inc.: Wallingford, CT, 2009.
(26) (a) Becke, A. D. Density-Functional Thermochemistry. I. The Effect of the Exchange-Only Gradient Correction. *J. Chem. Phys.* **1992**, *96*, 2155−2160. (b) Becke, A. D. Density-Functional Thermochemistry. II. The Effect of the Perdew−Wang Generalized-Gradient Correlation Correction. *J. Chem. Phys.* **1992**, *97*, 9173−9177. (c) Becke, A. D. Density-Functional Thermochemistry. III. The Role of Exact Exchange. *J. Chem. Phys.* **1993**, *98*, 5648−5652.
(27) Lee, C.; Yang, W.; Parr, R. G. Development of the Colle−Salvetti Correlation-Energy Formula into a Functional of the Electron Density. *Phys. Rev.* **1988**, *B37*, 785−789.
(28) Gonzalez, C.; Schlegel, H. B. An Improved Algorithm for Reaction Path Following. *J. Phys. Chem.* **1989**, *90*, 2154−2161.
(29) Lee, T. J.; Scuseria, G. In *Quantum-mechanical Electronic Structure Calculations with Chemical Accuracy*; Langhoff, S. F., Ed.; Kluwer: Dordrecht, Netherlands, 1995.
(30) Knowles, P. J.; Hampel, C.; Werner, H.-J. Coupled Cluster Theory for High Spin, Open Shell Reference Wave Functions. *J. Chem. Phys.* **1993**, *99*, 5219−5227.
(31) Martin, J. M. L.; Uzan, O. Basis Set Convergence in Second-Row Compounds. The Importance of Core Polarization Functions. *Chem. Phys. Lett.* **1998**, *282*, 16−24.
(32) (a) Klippenstein, S. J.; Marcus, R. A. High Pressure Rate Constants for Unimolecular Dissociation/Free Radical Recombination: Determination of the Quantum Correction via Quantum Monte Carlo Path Integration. *J. Chem. Phys.* **1987**, *87*, 3410−3417. (b) Klippenstein, S. J. Implementation of RRKM Theory for Highly Flexible Transition States with a Bond Length as the Reaction Coordinate. *Chem. Phys. Lett.* **1990**, *170*, 71. (c) Klippenstein, S. J. Variational Optimizations in the Rice−Ramsperger−Kassel−Marcus Theory Calculations for Unimolecular Dissociations with No Reverse Barrier. *J. Chem. Phys.* **1992**, *96*, 367−371. (d) Klippenstein, S. J. An Efficient Procedure for Evaluating the Number of Available States within a Variably Defined Reaction Coordinate Framework. *J. Phys. Chem.* **1994**, *98*, 11459−11464.
(33) (a) Wardlaw, D. M.; Marcus, R. A. RRKM Reaction Rate Theory for Transition States of Any Looseness. *Chem. Phys. Lett.* **1984**, *110*, 230−234. (b) Wardlaw, D. M.; Marcus, R. A. Unimolecular Reaction Rate Theory for Transition States of Partial Looseness. II. Implementation and Analysis with Applications to NO_2 and C_2H_6 Dissociations. *J. Chem. Phys.* **1985**, *83*, 3462−3480.
(34) Klippenstein, S. J.; Wagner, A. F.; Dunbar, R. C.; Wardlaw, D. M.; Robertson, S. H. *VARIFLEX*, version 1.00; Argonne National Laboratory: Argonne, IL, 1999.
(35) Hehre, W. J.; Ditchfield, R.; Radom, L.; Pople, J. A. Molecular Orbital Theory of the Electronic Structure of Organic Compounds. V. Molecular Theory of Bond Separation. *J. Am. Chem. Soc.* **1970**, *92*, 4796−4801.
(36) Radom, L.; Hehre, W. J.; Pople, J. A. Molecular Orbital Theory of the Electronic Structure of Organic Compounds. VII. Systematic Study of Energies, Conformations, and Bond Interactions. *J. Am. Chem. Soc.* **1971**, *93*, 289−300.
(37) Hehre, W. J.; Radom, L.; Schleyer, P. v. R.; Pople, J. A. *Ab Initio Molecular Orbital Theory*; John Wiley & Sons: New York, 1986.
(38) Minkin, V. I. Glossary of Terms Used in Theoretical Organic Chemistry. *Pure Appl. Chem.* **1999**, *71*, 1919−1981.
(39) Chase, M. W., Jr. *NIST-JANAF Thermochemical Tables*, 4th ed.; American Chemical Society: Washington, DC, American Institute of Physics for the National Institute of Standards and Technology: Woodbury, New York, 1998.

(40) Clifford, E. P.; Wenthold, P. G.; Lineberger, W. C.; Petersson, G. A.; Broadus, K. M.; Kass, S. R.; Kato, S.; DePuy, C. H.; Bierbaum, V. M.; Ellison, G. B. Properties of Diazocarbene [CNN] and the Diazomethyl Radical [HCNN] via Ion Chemistry and Spectroscopy. *J. Phys. Chem. A* **1998**, *102*, 7100−7112.
(41) Mebel, A. M.; Morokuma, K.; Lin, M. C. Modification of the GAUSSIAN-2 Theoretical Model: The Use of Coupled-Cluster Energies, Density-Functional Geometries, and Frequencies. *J. Chem. Phys.* **1995**, *103*, 7414−7421.
(42) Choi, H.; Mordaunt, D. H.; Bise, R. T.; Taylor, T. R.; Neumark, D. M. Photodissociation of Triplet and Singlet States of the CCO Radical. *J. Chem. Phys.* **1998**, *108*, 4070−4078.
(43) Mourits, F. M.; Rummens, F. H. A. A Critical Evaluation of Lennard−Jones and Stockmayer Potential Parameters and of Some Correlation Methods. *Can. J. Chem.* **1977**, *55*, 3007−3020.
(44) Baulch, D. L.; Cobos, C. J.; Cox, R. A.; Frank, P.; Hayman, G.; Just, Th.; Kerr, J. A.; Murrells, T.; Pilling, M. J.; Troe, J.; Walker, R. W.; Warnatz, J. Evaluated Kinetic Data for Combustion Modeling. Supplement I. *J. Phys. Chem. Ref. Data* **1994**, *23*, 847−848.